Accepted Manuscript

Temperature dependence of the Raman spectrum of 1-(4-chlorophenyl)-3-(2-thienyl)prop-2-en-1-one

T.A. de Toledo, R.C. da Costa, H.M. Al-Maqtari, J. Jamalis, P.S. Pizani

PII: S1386-1425(17)30162-2
DOI: doi: 10.1016/j.saa.2017.02.051
Reference: SAA 14973

To appear in: *Spectrochimica Acta Part A: Molecular and Biomolecular Spectroscopy*

Received date: 21 September 2016
Revised date: 13 February 2017
Accepted date: 22 February 2017

Please cite this article as: T.A. de Toledo, R.C. da Costa, H.M. Al-Maqtari, J. Jamalis, P.S. Pizani , Temperature dependence of the Raman spectrum of 1-(4-chlorophenyl)-3-(2-thienyl)prop-2-en-1-one. The address for the corresponding author was captured as affiliation for all authors. Please check if appropriate. Saa(2017), doi: 10.1016/j.saa.2017.02.051

Temperature dependence of the Raman spectrum of 1-(4-Chlorophenyl)-3-(2-thienyl)prop-2-en-1-one

T. A. de Toledo[a, b, *], R. C. da Costa[a,c], H. M. Al-Maqtari[d], J. Jamalis[d], P. S. Pizani[a]

[a] Universidade Federal de São Carlos, Departamento de Física, São Carlos-SP, 13565-905, Brazil.

[b] Universidade de Cuiabá, Faculdade de Engenharia, Campus Barão, Cuiabá - MT, 78005-300, Brazil.

[c] Universidade Federal de Campina Grande, Centro de Ciências e Tecnologia Agroalimentar, Pombal-PB, 58840-000, Brazil.

[d] Universiti of Teknologi Malaysia, Department of Chemistry, Faculty of Science, Malaysia.

Abstract

The heterocyclic chalcone containing thiophene ring 1-(4-Chlorophenyl)-3-(2-thienyl)prop-2-en-1-one, $C_{13}H_9ClOS$ was synthesized and investigated using experimental techniques such as nuclear magnetic resonance (^1H and ^{13}C NMR), Fourier transform infrared spectroscopy (FTIR) at room temperature, differential scanning calorimeter (DSC) from room temperature to 500 K and Raman scattering at the temperature range 10-413 K in order to study its structure and vibrational properties as well as stability and possible phase transition. Density functional theory (DFT) calculations was performed to determine the vibrational spectrum viewing to improve the knowledge of the material properties. A reasonable agreement was observed between theoretical and experimental Raman spectrum taken at 10 K since anharmonic effects of the molecular motion is reduced at low temperatures, leading to a more comprehensive assignment of the vibrational modes. Increasing the temperature up to 393 K, was observed the typical phonon anharmonicity behavior associated to changes in the Raman line intensities, line-widths and red-shift, in special in the external mode region, whereas the internal modes region remains almost unchanged due its strong chemical bonds. Furthermore, $C_{13}H_9ClOS$ goes to melting phase transition in the temperature range 393-403 K and then sublimates in the temperature range 403-413 K. This is denounced by the disappearance of the external modes and the absence of internal modes in the Raman spectra, in accordance with DSC curve. The enthalpy (ΔH) obtained from the integration of the endothermic peak in DSC curve centered at 397 K is founded to be 121.5 J/g.

Keywords: Heterocyclic; 1-(4-Chlorophenyl)-3-(2-thienyl)prop-2-en-1-one; Spectroscopic studies; Phase transition; Phonon Anharmonicity; DFT calculations.

---

* Corresponding author. Phone: (55) 65 99981-3753;

E-mail address: thiagotoledo21@gmail.com

1. Introduction

The investigation of temperature dependence of the Raman spectrum of the organic materials, in special those with potential biological application, has attracted the attention of many studies in the last decades because the vibrational spectrum plays a fundamental role in material properties like thermal expansion, anharmonicity, stability and phase transition [1-3]. For example, in the case of pharmaceuticals, any change in the molecular structure may lead to modification in the biological properties, therefore is essential to determine the temperature stability range in order to avoid risk to human life [4,5]. On the other hand, in the case of electronic device applications, the understanding of electron-phonon interaction, transport and vibrational properties due to heating is also a relevant matter because of technological driver such as nanoparticles for thermal medical therapies and thermal management of nanoscale electronic devices [6, 7]. Usually, this information may be revealed by band position and line broadening in the Raman spectrum when temperature increases.

In the view of mentioned facts and our concern on the investigation of the thermal properties of organic materials, the heterocyclic chalcone containing thiophene ring 1-(4-Chlorophenyl)-3-(2-thienyl)prop-2-en-1-one, $C_{13}H_9ClOS$ is synthesized and investigated using the experimental technique such as nuclear magnetic resonance (^{1}H and ^{13}C NMR), Fourier transform infrared spectroscopy (FTIR) at room temperature, differential scanning calorimeter (DSC) from room temperature to 500 K and Raman scattering technique in the temperature range 10-413 K in order to investigate its molecular structure, vibrational properties, stability and a possible phase transition, which is a fundamental parameter for technological application. To improve the knowledge of the physical properties of this material, theoretical calculation based on density functional theory (DFT) is performed viewing to predict the most of vibrational

modes and then correlating with the experimentally observed infrared and Raman bands, that is, the theoretical predictions serves as a guide to understand the vibrational spectrum. To the best of our knowledge, there is limited information available in the literature about $C_{13}H_9ClOS$ properties, with exception of the crystalline structure determination at low temperature available in ref. [8], which also motivates this investigation. According to literature [9-15], thiophene and chalcone derivatives exhibit several biological properties, among others, antibacterial and anticancer activities as well as shows a potential application in optical devices because of the large nonlinear optical coefficient due its conjugated π-electrons. It is also appropriate to mention that the presence of double bond in conjunction with carbonyl group in the molecular structure of chalcone derivatives is responsible for their biological properties [11,12], meanwhile the C=C-S nucleus is associated to biological activities of thiophene derivatives [9]. Furthermore, it is supposed that the combination of chalcones with heterocyclic thiophene ring may increases the biological activities of chalcone derivatives [16].

2. Experimental Procedures

2.1 – Synthesis process

$C_{13}H_9ClOS$ was synthesized according to chemical procedure described in the literature [15], as displayed in Figure 1. A mixture of 4-chloroacetophenone (**1**) (0.02 mol) with thiophene-2-carbaldehyde (**2**) (0.02 mol) was dissolved in methanol 25 mL, aqueous potassium hydroxide 15 mL was added drop wise. The reaction mixture was stirred at room temperature overnight and then the solid product was separated, washed, dried to obtain the organic compound (**3**). The crystal used in Raman experiment was growth by slow evaporation of room temperature of methanol solution of (**3**).

2.2 – Measurements and experimental apparatus

^{1}H and ^{13}C NMR spectra (400 MHz and 300 MHz respectively) were recorded on Bruker Avance II spectrometer using deuterated chloroform ($CDCl_3$) as solvent. Chemical shift values were given in δ (ppm) scales. Thin layer chromatography (TLC) alumina sheets pre-coated with silica gel 60 F254 (0.2 mm thickness) was used to monitor and detect compounds and the spots were visualized under UV lamp at 254 nm. All chemicals and reagents were of analytical grade and were used without further purification. The infrared spectrum was recorded using potassium bromide (KBR) pellet method on Shimadzu 8000 series standard spectrometer in the spectral region 650-4000 cm^{-1} with spectral resolution of 4 cm^{-1}. The thermal properties of the $C_{13}H_9ClOS$ was characterized by differential scanning calorimetry (DSC) in Netzsch DSC 200 F3 Maia from room temperature to 500 K, at a heating rate of 5 K/min under argon atmosphere. The Raman scattering measurements were performed in a HR800 Evolution micro-Raman spectrometer from Horiba-Jobin-Yvon with a charge coupled device as light detector and the 633 nm line of a He-Ne laser as excitation source. The low-temperature measurements were performed in cryogenic closed system in the temperature range from 10 to 290 K. For the high temperature measurements (room temperature up to 433 K) were used a Linkan TS1500 micro furnace.

3. Computational Methods

Density functional theory (DFT) calculations were performed using B3LYP [17,18] method with 6-311G(d, p) basis set on ORCA software package [19]. The harmonic vibrational frequencies were calculated at optimized molecular structure and non-negative frequency was obtained. Therefore, in our calculations we have obtained a true minimum of potential energy. The Raman spectrum was obtained from the sum of

the Lorentzian functions with haft-band-width (HW) of 4 cm^{-1}. In addition, the Raman intensity given by DFT calculations were converted to relative intensity (I) using the expression derived from Raman scattering activity (S_i) theory, $I = 10^{-12}(\nu_0 - \nu_i)^4 \nu_i^{-1} S_i$, where ν_0 is the wavenumber of the laser source excitation and ν_i is the wavenumber normal mode [20]. The theoretical spectrum was scaled by scale factor of 0.98 and 0.978 in the spectral region below and above 1800 cm^{-1}, respectively, in order to best comparison with experimental Raman spectrum, because in our calculations the anharmonicity was neglected. Finally, the experimental Raman spectrum taken at 10 K was compared with theoretical one.

4. Results and Discussions

4.1. Molecular Structure

Figure 2 shows the ^1H and ^{13}C NMR spectra of $C_{13}H_9ClOS$. The ^1H NMR spectrum confirm the proposed structure due to the presence of six signals integrating for nine protons. For example, two olefinic protons of H-*α* and H-*β* appeared as doublet at 7.31 ppm and 7.98 ppm, respectively. In addition, trans-configuration of $C_{13}H_9OSCl$ is confirmed by coupling constant of vinylic protons (15.20 Hz). Moreover, the ^{13}C NMR spectrum revealed eleven signals for carbons in agreement with the proposed structure and also showed the chemical shift values of *α* and *β* carbons at δ 120.12 and δ 137.73 ppm, respectively. Furthermore, the appearance of the signal at δ 188.55 ppm corresponds to carbonyl group [21, 22]. Finally, the complementary analytical data of NMR spectra used to identify the molecular structure of $C_{13}H_9ClOS$ are: ^1H NMR (400 MHz, $CDCl_3$): δ 7.13 (dd, 1H, *J* = 3.6 Hz, *J* = 5.2 Hz, H-4), 7.31(d, 1H, *J* = 15.2 Hz, H-*α*), 7.40 (d, 1H, *J* = 3.6 Hz, H-3), 7.47 (d, 1H, *J* = 5.2 Hz, H-5), 7.50 (d, 2H, *J* = 8.6 Hz, H-‘3 and H-‘5), 7.96 (d, 1H, *J* =15.2 Hz, H-*β*), 7.98 (d, 2H, *J* =8.6 Hz, H-‘2 and H-‘6);

^{13}C NMR (75 MHz, $CDCl_3$): 120.12, 128.46, 128.96, 129.13, 129.83, 132.46, 136.41, 137.73, 139.21, 140.21, 188.55.

Figure 3 shows the optimized structure of $C_{13}H_9ClOS$ obtained with B3LYP/6-311G(d,p) method as well as atomic numbering scheme used in this study to describe the vibrational normal modes and the structural properties. The $C_{13}H_9ClOS$ molecule comprises two rings, named here as R1 and R2. R1 are formed by atoms C1 to C6, which comes from benzene ring. R2 are formed by atoms C10 to S1, which comes from thiophene ring. R1 and R2 are linked by enone chain (C9=C8-C7=O1). On table 1, the comparison between experimental data available in ref. [8] and calculated geometric parameters for $C_{13}H_9ClOS$ is listed. From this table, it is seen that the predicted bond distance and angle for $C_{13}H_9ClOS$ is comparable to analogous experimental one, with exception of the C10-C11 [1.382 Å], C11-C12 [1.415 Å], C10-S1 [1.753 Å], C13-S1 [1.723 Å], C9-C10-C11 [130.7º] and C12-C13-S1 [111.7º], since it exhibits a deviation value of 0.315 Å, 0.272 Å, 0.315 Å, 0.087 Å, 8.9º and 11.4º in relation to experimental data given in ref. [8], which may be explained by atomic substitution and disorder effect in thiophene ring, as discussed in ref. [8] and [23]. Another interesting features predicted by DFT calculations for $C_{13}H_9ClOS$ molecule is associated to the bond distance of carbon-carbon (C9-C8), carbonyl group (C7-O1) and carbon-chlorine (C2-Cl1) calculated to be 1.349, 1.225 and 1.755 Å. The first one is in close agreement with experimental and theoretical data reported in ref. [8] and [10], but present a deviation of 0.001/0.006 Å and 0.012/0.018 Å in relation to experimental data available in the literature for (2E)-1-(4-Chlorophenyl)-3-[4-(methylsulfanyl)phenyl]prop-2-en-1-one, $C_{16}H_{13}ClOS$ [24] and $C_{13}H_9ClOS$ [8], which is probably attributed to higher π-conjugation effect, as indicated by ref. [12] for analogous material. Furthermore, the bond angle of C3-C2-C1 and C4-C5-C6 in R1 calculated to be 121.2º and 118.5º

exhibits a small deviation of 0.62/0.74º and 1.16/0.61° in relation to experimental data available in ref. [8] and [24]. Finally, it is worth to mention that $C_{13}H_9ClOS$ is twisted about the C5-C7 bond with dihedral angle of -12.01º and -27.58º in relation to thiophene ring (C8-C9-C10-C11) and benzene ring (C6-C5-C7-C8), as displayed in ref. [8], in contrast to almost planar structure predicted by DFT calculations. This difference may be explained by the absence of the atomic packing factor and disorder of thiophene ring because DFT calculation is performed on isolated molecule of $C_{13}H_9ClOS$ without any constrain to potential energy surface (PES), whereas it crystalline structure belongs to triclinic structure, space group P-1, with two molecular formulas per unit cell as well as stabilized by intermolecular interactions ($C - H \cdots \pi$) involving R1 and R2 [8].

4.2. Vibrational Analysis

Figure 4 shows the theoretical and experimental Raman spectra of the $C_{13}H_9ClOS$ recorded at 10 K with a reasonable accordance between them, in especial because at low temperature the anharmonic effects of the molecular motion is reduced, leading to more comprehensive vibrational spectrum. In the experimental spectrum, it is observed two different types of vibrational motions, since in the molecular crystal the force between molecules, which is responsible to link between molecules in the solid state, is weak compared to the intramolecular. Therefore, the external modes usually arise in the vibrational spectrum in lower frequencies relationship to internal modes [26, 27]. In this context, the first spectral region (in the range 10-200 cm^{-1}) is associated to external modes in which molecules in the unit cell moves relatives to one another in phase, whereas the second one (in the range ~280-3200 cm^{-1}) is attributed to functional group modes like stretching (ν), in-plane (δ) and out-of-plane (γ) bending vibrational modes of C-C, C-O and C-H and skeletal torsion (τ) modes, as listed in Table 2. In order to illustrate the normal mode description given in this study, the wave vector

displacement for four selected vibrational normal modes from isolated molecular structure of $C_{13}H_9ClOS$ is presented in Figure 5.

In the phonon spectrum, it is seen 13 external modes centered at 21, 34, 43, 51, 60, 79, 93, 105, 124, 139, 147, 155 and 196 cm^{-1}. According to DFT calculations, this vibrational motion is described as molecular torsion modes relationship to equilibrium position of the molecule. On the other hand, in the internal mode region, the characteristic band associated to vibrational motion of the para-substituted benzene is usually reported in the vibrational spectrum near 1415 and 1515 cm^{-1} [28]. Thus, the Raman band centered at 1417 and 1518 cm^{-1} in the vibrational spectrum of $C_{13}H_9ClOS$ is attributed to benzene substitution pattern and assigned as C=C stretching coupling with CH bending mode, in close agreement with theoretical description. In the infrared spectrum of the $C_{13}H_9ClOS$, these vibrational mode arises at 1421 and 1510 cm^{-1}, as it can be observed in supplementary file. The stretching mode of C=O and C=C is seen in vibrational spectrum of chalcone derivatives [15, 29], respectively, in the range 1850-1600 cm^{-1} and 1625-1575 cm^{-1}. For (2E)-3-[4-(methylsulfanyl)phenyl]-1-(4-nitrophenyl)prop-2-en-1-one this vibrational mode is observed near 1655 and 1583 cm^{-1} [14, 16]. In the case of $C_{13}H_9ClOS$, these vibrational mode arises in the Raman spectrum at 1584, 1591 and 1653 cm^{-1}, while in the infrared spectrum at 1565, 1582 and 1652 cm^{-1}. According to DFT calculations, these vibrational modes are described as mix mode composition of ν(C=O) coupled to ν(C=C) and CH bending and is predicted at 1596 and 1675 cm^{-1}. It is relevant to mention that the weak intensity Raman line at 1653 cm^{-1} is may be associated to C=O substitution effect in benzene ring, in contrast to medium-strong band in the infrared spectrum viewed at the 1652 cm^{-1}. Another interesting contribution in the vibrational spectrum of the $C_{13}H_9ClOS$ is related to thiophene ring vibrational motion. The semi-circle and quadrant stretching together with CH bending

in thiophene ring is reported in ref. [28, 30] near 1357, 1408 and 1588 cm^{-1}, respectively. In the Raman spectrum of $C_{13}H_9ClOS$, the latter is associated to the band centered at 1361 and 1425 cm^{-1}, while appears at 1358, 1410 and 1583 cm^{-1} in the infrared spectrum. Moreover, many of the bands seen in the vibrational spectrum of the aromatic rings in the spectral region 1300-620 cm^{-1} involve in-plane and out-of-plane CH bending vibrations mixed with C-C stretching and C-C-C bending vibrations [16, 28]. For example, the in-plane CH bending of benzene ring is reported at 1037, 1146 and 1178 cm^{-1}, while the out-of-plane CH bending at 673, 846 and 990 cm^{-1} [28]. For this reason, the band centered around at 1078, 1092, 1109 and 1179 cm^{-1} in the Raman and infrared spectrum of the $C_{13}H_9ClOS$ is assigned as in-plane CH bending, δ(CH), while the band located proximally at 874, 955, 970 and 979 cm^{-1} is attributed to out-of-plane CH bending mode, γ(CH), in agreement with theoretical description. For thiophene ring, the in-plane CH bending arises in the vibrational spectrum at 1036, 1083, 1085 and 1256 cm^{-1}, while the out-of-plane CH bending appears at 683, 867 and 898 cm^{-1} [30]. Thus, the Raman (infrared) band near 1029 (1031), 1045 (1049), 1135 (113) and 1216 (1210) cm^{-1} is assigned as in-plane CH bending, whereas the band centered at 679 (673) and 892 (889 and 912) cm^{-1} is attributed to out-of-plane CH bending. According to DFT calculations, the first vibrational mode is predicted at 1014, 1046, 1080, 1128 and 1247 cm^{-1}, while the second one at 814, 818 and 902 cm^{-1}. Furthermore, to complete the tentative assignment of the vibrational mode of $C_{13}H_9ClOS$, it is discussed the CH stretching mode of benzene and thiophene ring common reported in the region 3000-3200 cm^{-1} [25, 28, 30]. In the Raman spectrum of $C_{13}H_9ClOS$, it is observed six bands with very low intensity near 3020, 3059, 3074, 3086, 3109 and 3111 cm^{-1}, whereas in the infrared spectrum it is seen five bands proximally at 3075, 3080, 3083, 3100 and 3200 cm^{-1} also with very low intensity. In particular, the band centered at 3059, 3086

and 3111 cm^{-1} is described by DFT calculations as a vibrational contribution of ν(C8H5) + ν(C6H4) + ν(C1H1), $ν_{R1}$(CH) + ν(C8H5) and ν(C13H9), respectively.

4.4. Temperature dependence on Raman spectra

Figure 6 shows the Raman spectra of the $C_{13}H_9ClOS$ in the temperature range 10-413 K, in the lattice mode region. Increasing temperature from 10 K to 393 K, it can be observed a red-shift, change in the line-width and relative intensity of some external modes, while the internal modes remain almost unchanged with temperature. For organic crystals, this effect is, in general, attributed to phonon anharmonicity as well as to the nature of the chemical bond (intra- and inter-molecular). For example, it is seen the coalescence of the Raman band in external and internal modes region with increasing temperature, as shown in Fig. 6 and 7, described as: (i) the band located at 46 and 53 cm^{-1} (at 10 K) assign as lattice modes becomes a asymmetric band centered at 42 cm^{-1} in the temperature range 200-300 K; (ii) the band at 80 cm^{-1} also attributed to lattice mode exhibits loss in intensity and moves more faster that the intensity at 57 cm^{-1} which leads to the coalescence of both at 393 K; (iii) the low intensity band at 93 cm^{-1} presents loss in intensity as temperature increase and becomes a shoulder with a very low intensity of the band near 96 cm^{-1} in the Raman spectrum taken at room temperature; (iv) the Raman band associated to stretching of C=C coupled with CH bending near 1416 and 1424 cm^{-1} (indicated by down-arrow) becomes a single band near 1421 cm^{-1} at 403 K, and (v) the shoulder located at 1593 cm^{-1} associated to mix mode composition of ν(C=O) + ν(C=C) + δ(CH), moves more fast than the intensity line at 1585 cm^{-1} which leads to the coalescence of both at room temperature. These thermal events are characteristic of phonon anharmonicity contribution to inter-atomic potential. However, a great modification in the Raman spectra profile occurs in the temperature range 393-413 K. The first change is associated to the melting of the

molecular crystal $C_{13}H_9ClOS$. This phenomenon, seen proximally at 403 K, is explained by fact the that the external mode region becomes similar to Rayleigh line tail. At the same time, in the internal mode region, several of the weaker bands could not be resolved from their background or their position could not be determined reliable, with exception of the vibrational modes attributed to C=C stretching coupling with CH bending mode of benzene and thiophene rings, which arise in the spectral region 1350-1700 cm^{-1}. The latter may be associated with the phase transition induced by temperature, in concordance with DSC curve, as illustrated in Fig. 8. In addition, a discontinuity in **dω/dt** strongly suggest a possible phase transition, as indicated in the literature [1] for the Salophen crystals. Moreover, near the temperature of 413 K, a second change occurs in the Raman spectrum associated to crystal sublimation. This thermal event is supported by the endothermic peak in the DSC curve centered at 397 K whose enthalpy energy is founded to be 121.5 J/g. Furthermore, after cooling to room temperature (*300 K), it was observed the crystallization of the organic substance in the optic window of the furnace. In this sense, a new Raman spectrum was taken in order to compare to initial one. As expected, no significant modification is observed the internal modes region, therefore no change occurs in the molecular structure of the 1-(4-Chlorophenyl)-3-(2-thienyl)prop-2-en-1-one, $C_{13}H_9ClOS$ as displayed in figure 7 (a-d). However, in the external mode region, the downshift and different intensity of the band centered at 17, 29, 45 and 61 cm^{-1} (marked with down arrow) relationship to initial spectrum taken at room temperature suggests a change of the atomic force constant, as can be seen in the figure 6 (b).

Conclusions

In this study, the structural and vibrational properties of the 1-(4-Chlorophenyl)-3-(2-thienyl)prop-2-en-1-one, $C_{13}H_9ClOS$ were investigated combining experimental

techniques such as nuclear magnetic resonance (^{1}H NMR and ^{13}C NMR), Fourier transform infrared (FTIR) spectroscopy at room temperature, differential scanning calorimeter (DSC) from room temperature to 500 K and Raman scattering in the temperature 10-413 K with theoretical calculation based on density functional theory in order to describe the vibrational spectrum, to determine the temperature stability and a possible phase transition. A detailed description of vibrational normal modes is given for $C_{13}H_9ClOS$ in terms of experimental results of analogous compounds and DFT calculation. The phonon anharmonicity contribution to inter-atomic potential is observed in the Raman spectrum in all temperature range 10-393 K and is related to change in Raman line (broadening and shift). The phase transition from solid to liquid, attributed to disappearance of all external modes, was observed around at 403 K, followed by sublimation of the molecular crystal in the temperature range 403-413 K, as also indicated by the endothermic peak in DSC curve centered at 397 K with thermal energy for the sublimation temperature of the 121.5 J/g. Furthermore, the line intensity and shift in the Raman spectra taken after cooling (*300 K) indicates a possible change of the atomic force constant of the material. Finally, this study provides a fundamental support to understand origin of lattice instability and improves the knowledge of the physical properties of the investigated material.

Acknowledgments

The Brazilian authors would like to acknowledge the agencies CNPQ and FAPESP (grant 2013/07793-6) for financial support. Joazaizulfazli Jamalis wish to thank the Ministry of Higher Education (MOHE) for funding this research under the Research University Grant (RUP) with vote No. 07J48, and the Fundamental Research Grant Scheme (FRGS) with vote No. 4F448.

References

[1] T. A. de Toledo, R.C. da Costa, L.E. da Silva, A.M.R. Teixeira, V.N. Lima, D.M. Sena Jr., H.D. Melo Coutinho, P.T.C. Freire, P.S. Pizani. J. Mol. Struct. 1115 (2016) 105-108.

[2] R. J. C. Lima, P. T. C. Freire, J. M. Sasaki, F. E. A. Melo, J. Mendes Filho, R. L. Moreira. J. Raman Spectrosc. 32 (2001) 751–756.

[3] I. C. V. Bento, P. T. C. Freire, R. R. F. Bento, V. Lemos, F. E. A. Melo, J. Mendes Filho, P. S. Pizani, A. J. D.Moreno. *J. Raman Spectrosc.* 37 (2006) 1393–1397.

[4] A. P. Ayala, S. B. Honorato, J. Mendes Filho, D. Grillo, M. Quintero, F. Gilles, G. Polla. Vib. Spectrosc. 54 (2010) 169–173.

[5] M. Sardo, A. M. Amado, P. J. A. Ribeiro-Claro. J. Raman Spectrosc. 39 (2008) 1915-1924.

[6] P.Y. Yu, M. Cardona. Fundamentals of Semiconductors. 3ª Ed. Springer, 2001.

[7] D. G. Cahill et al., Appl. Phys. Rev. 1, 011305 (2014).

[8] Shea-Lin Ng et al., Acta Cryst. E62 (2006) o3200–o3202.

[9] R. Mishra, K. K. Jha, S. Kumar, I. Tomer. Der Pharma Chemica, 2011, Vol. 3, pp. 38-54.

[10] V. N. Gogte, L. G. Shah and B. D. Tilak. Tetrahedron 23 (1967) 2437-2441.

[11] P. Singh, A. Anand, V. Kumar. E. J. Med. Chem. 85 (2014) 758-777.

[12] Amit Kumar, Vipin Deval, Poonam Tandon, Archana Gupta, E. Deepak D'silva. Spectrochimica Acta Part A: Molecular and Biomolecular Spectroscopy 130 (2014) 41–53.

[13] C-P Chen, S-H Chan, T-C Chao, C. Ting, B-T Ko. J. AM. CHEM. SOC. 2008, *130*, 12828–12833.

[14] E.D. D'silva, D.Narayan Rao, Reji Philip, Ray J. Butcher, Rajnikant, S.M.Dharmaprakash. J Phys Chem of Solids 72 (2011) 824–830.

[15] Z. Mokhtar, J. Jamalis, S. P. M. Bohari, M. M. Rosli, H-K. Fun. Molecular Crystals and Liquid Crystals, 2016, Vol. 631, pp. 119-131.

[16] C. S. C. Kumar, C. Parlak, H-K. Fun, M. Tursun, G. Kesan, S. Chandraju, C. K. Quah. Spectrochimica Acta Part A: Molecular and Biomolecular Spectroscopy 127 (2014) 67–73.

[17] A.D. Becke, Physical Review A, 38 (1988) 3098-3100.

[18] C. Lee, W. Yang, R.G. Parr, Physical Review B, 37 (1988) 785-789.

[19] Neese, Frank (2012). "The ORCA program system". Wiley Interdisciplinary Reviews: Computational Molecular Science 2 (1): 73–78.

[20] T.A. de Toledo, L.E. da Silva, T.C. Botelho, R.J. Ramos, P.T. de Souza Jr, A.M.R. Teixeira, P.T.C. Freire, R.R.F. Bento, J. Mol. Struct., 1029 (2012) 22-27.

[21] D.L. Pavia, G.M. Lampman, G.S. Kriz, J.R. Vyvyan, Introduction to Spectroscopy, Fourth ed., Cenage Learning, 2009.

[22] R.M. Silverstein, F.X. Webster, D.J. Kiemle, Spectrometric Identification of Organic Compounds, 7th ed., John Wiley & Sons, 2005.

[23] T. Kupka, R. Wrzalik, G. Pasterna, K. Pasterny. J. Mol. Struct. 616 (2002) 17-32.

[24] William T. A. Harrison, H. S. Yathirajan, B. Narayana, A. Mithun, B. K. Sarojini, *Acta Crystallographica, Section E* (2006), **62**, o5290.

[25] B. K. Sarojini, H. S. Yathirajan, K. Mustafa, H. Sarfraz, M. Bolte, *Acta Crystallographica, Section E* (2007), **63**, o4448.

[26] T.A. de Toledo, L.E. da Silva, A.M.R. Teixeira, P.T.C. Freire, P.S. Pizani. J. Mol. Struct. 1091 (2015) 37–42.

[27] M. Ito, T. Shigeoka. Spectrochimica Acta 22 (1966) 1029-1044.

[28] P. J. Larkin. IR and Raman Spectroscopy: Principles and Spectral Interpretation. Elsiever, 2011.

[29] A.M. Asiri, M. Karabacak, S. Sakthivel, A.O. Al-youbi, S. Muthu, S.A. Hamed, S. Renuga, T. Alagesan. J. Mol. Struct. 1103 (2016) 145-155.

[30] M. Rico, J. M. Orza, J. Morcillo. Spectrochimica Acta 21 (1965) 689-719.

Figure Captions

Fig. 1: Chemical procedure used to synthetize the organic compound (E)-1-(4-Chlorophenyl)-3-(thiophen-2-yl)prop-2-en-1-one, $C_{13}H_9OSCl$.

Fig. 2: ^{1}H and ^{13}C NMR spectra of the $C_{13}H_9OSCl$.

Fig. 3: Optimized structure of $C_{13}H_9OSCl$ molecule obtained with B3LYP/6-311G(d,p) method.

Fig. 4: Theoretical and experimental Raman spectra of the $C_{13}H_9OSCl$ taken at 10 K.

Fig. 5: Selected Raman modes for 1-(4-Chloro-phenyl)-3-thiophen-2-yl-propenone molecule calculated with B3LYP/6-311G(d,p) method: (a) C-H bending in benzene ring at 1201 cm^{-1}, (b) δ(C13H9) + δ(C12H8) + δ(C11H7) at 1272 cm^{-1}, (c) ν(C=C) + δ(CH) at 1390 cm^{-1} and (d) ν(C=O) + ν(C=C) + δ(CH) at 1629 cm^{-1}.

Fig. 6: Raman spectra of $C_{13}H_9OSCl$ in the external mode region (a) in the temperature range 10-300 K (b) in the temperature range 313-403 K.

Fig. 7: Raman spectra of $C_{13}H_9OSCl$ in the temperature range 10-433 K and spectral region (a) 300-650 cm^{-1}, (b) 650-1250 cm^{-1}, (c) 1250-1675 cm^{-1} and (d) 2900-3200 cm^{-1}. The dash is only for guide the eye.

Fig. 8: DSC thermogram for $C_{13}H_9OSCl$ in the temperature range 350-420 K.

Table Captions

Table 1: Experimental [8] and calculated geometric parameters for 1-(4-Chloro-phenyl)-3-thiophen-2-yl-propenone, $C_{13}H_9ClOS$: bond distance, bond angle and dihedral angle (Å, °).

Table 2: Experimental and theoretical Raman modes for 1-(4-Chloro-phenyl)-3-thiophen-2-yl-propenone along with their description.

Figure 1

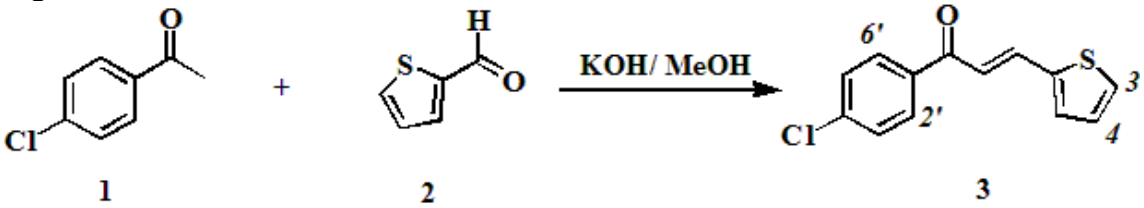

Figure 2

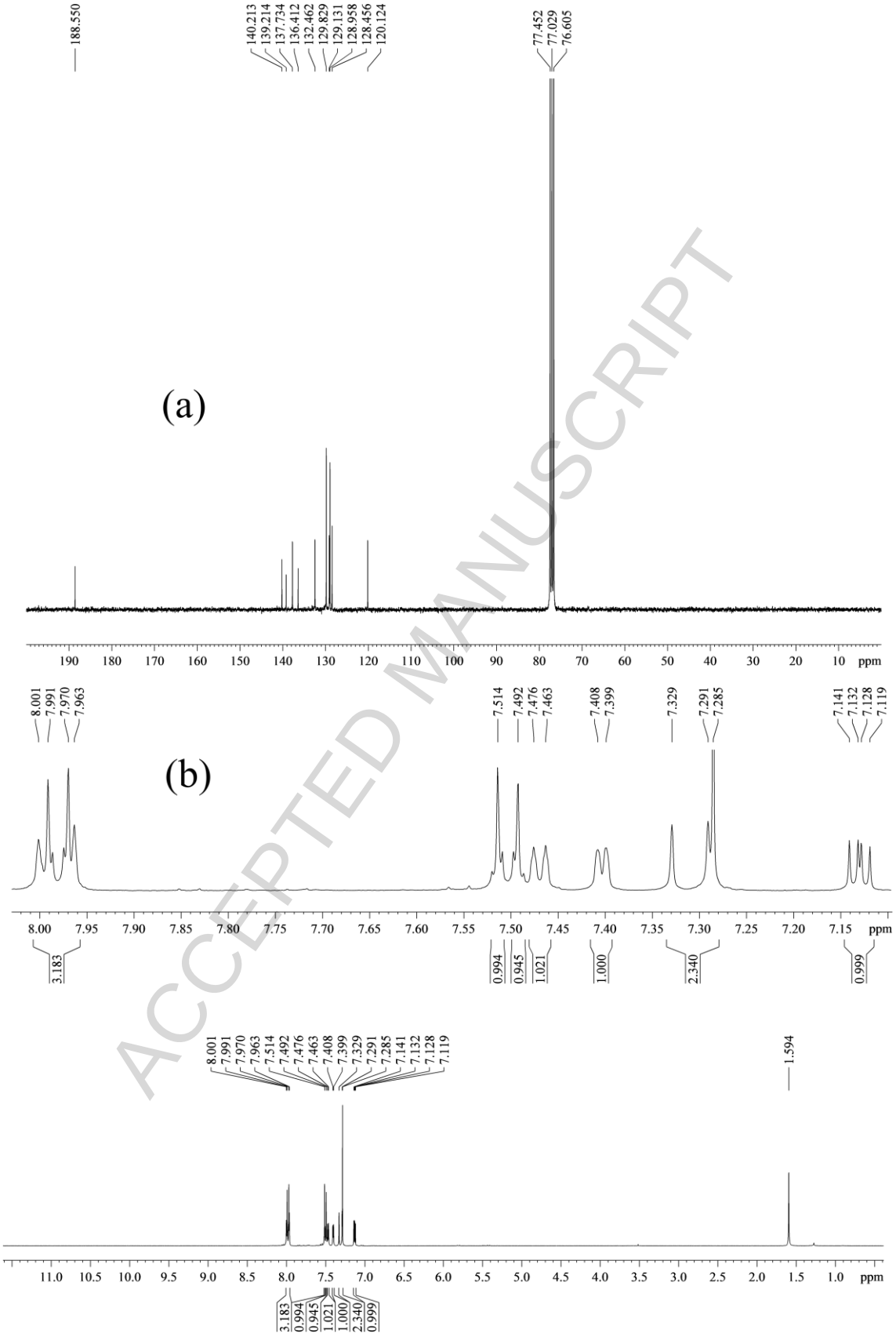

Figure 3

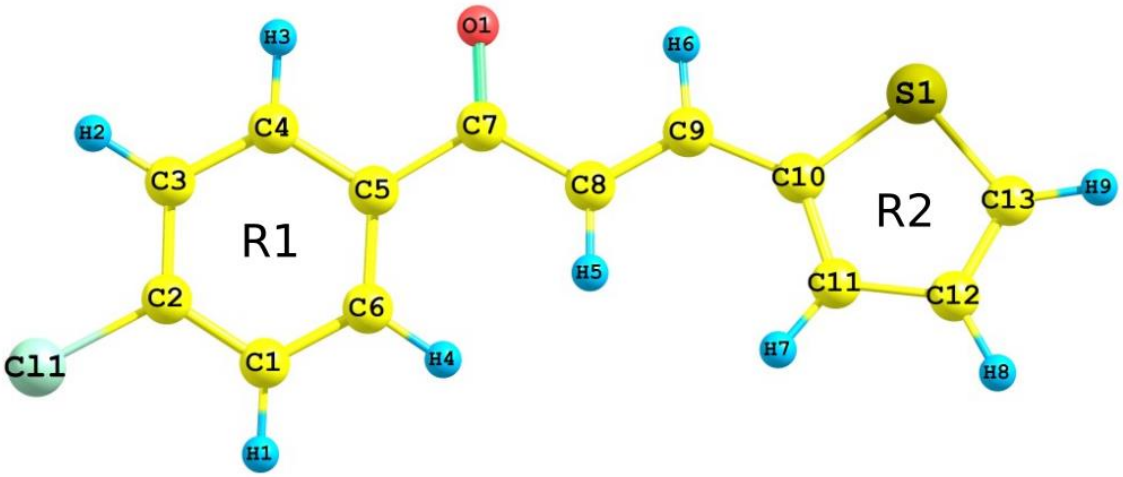

Figure 4

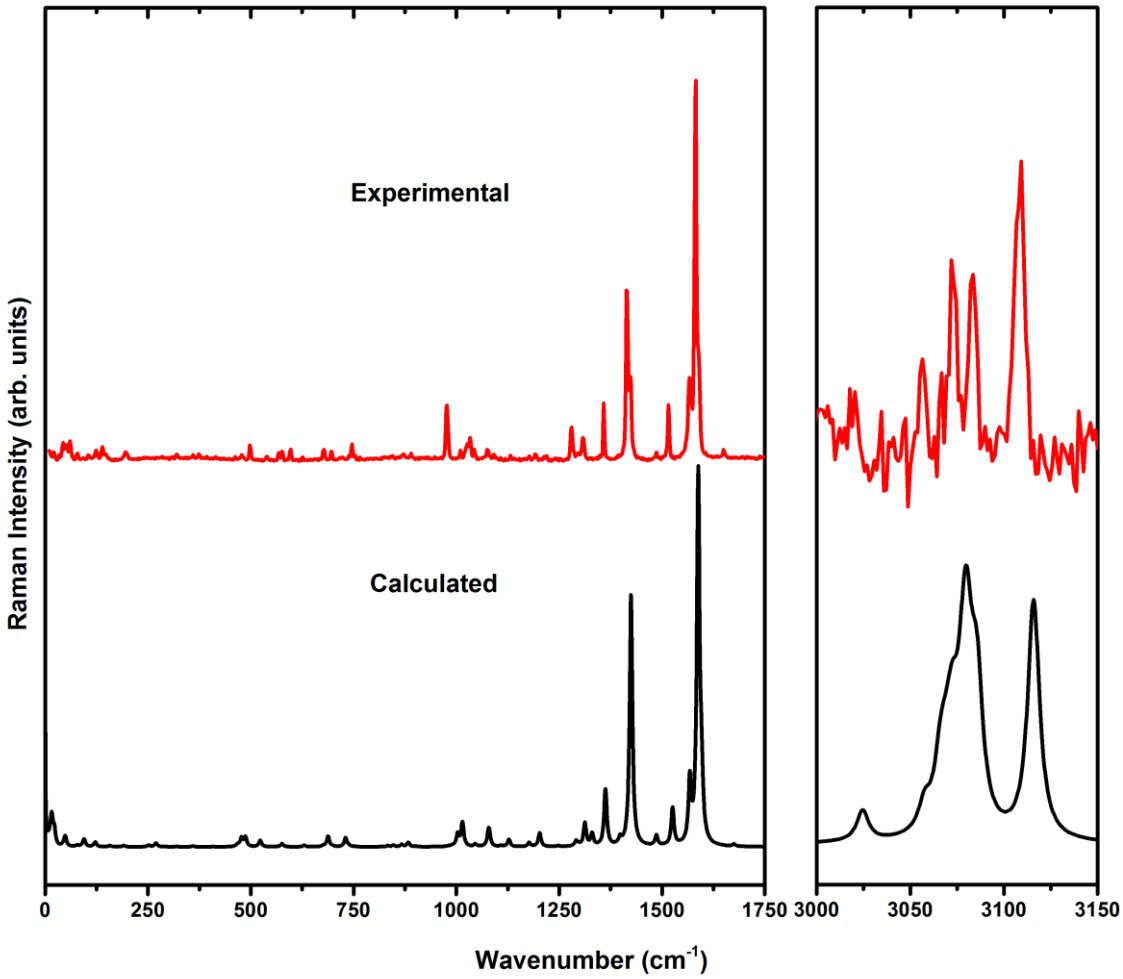

Figure 5

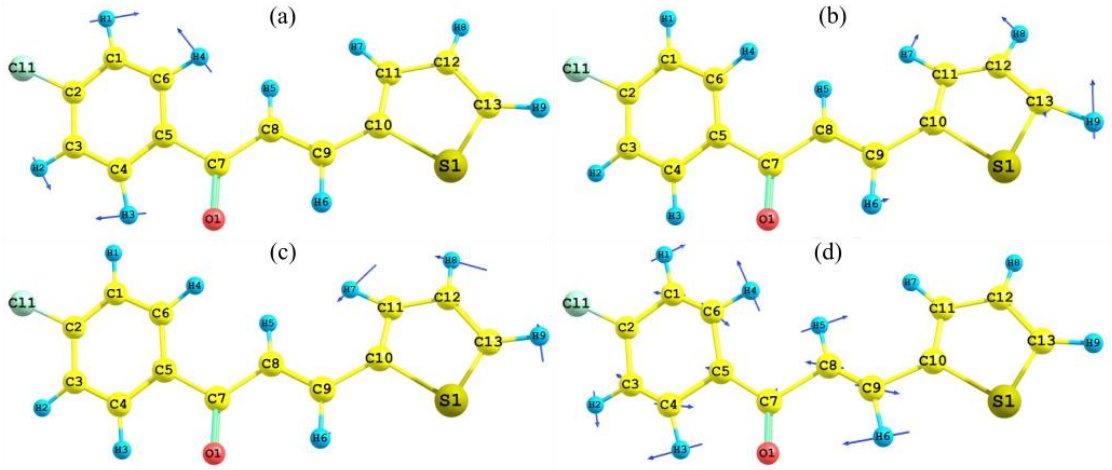

Figure 6

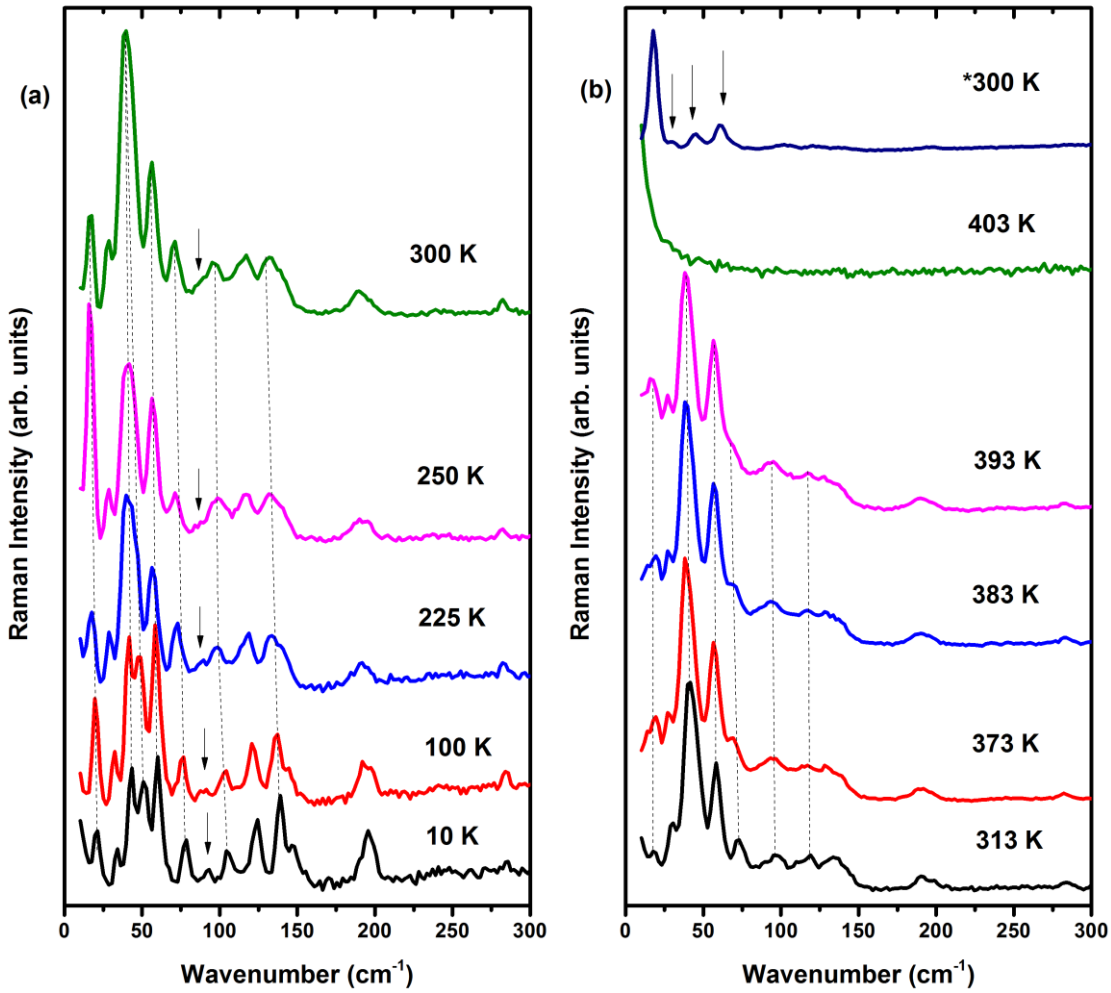

Figure 7

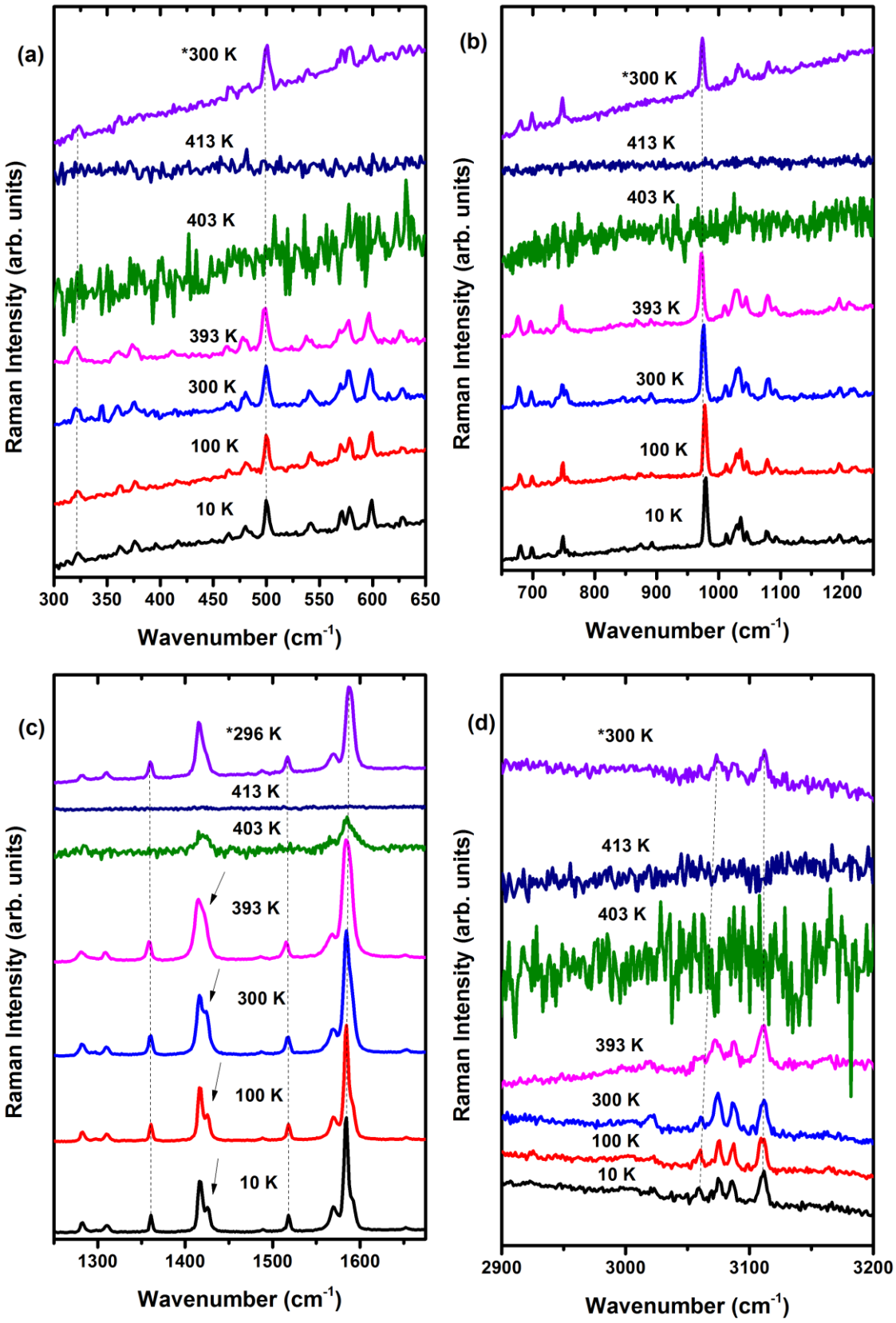

Figure 8

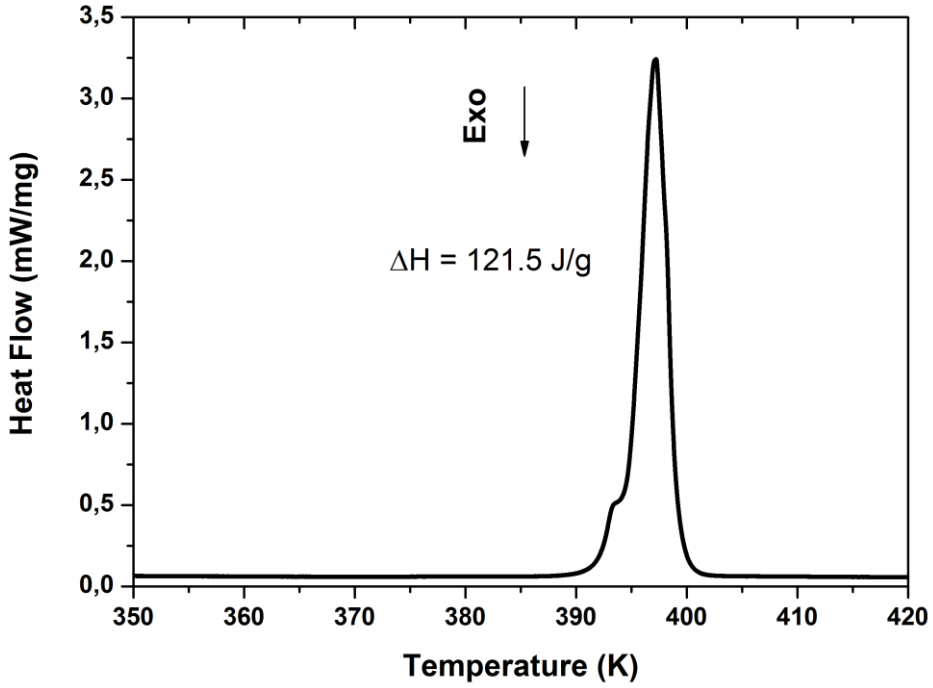

Table 1: Experimental[1] and calculated geometric parameters for 1-(4-Chloro-phenyl)-3-thiophen-2-yl-propenone, $C_{13}H_9ClOS$: bond distance, bond angle and dihedral angle (Å, º).

Atom name	Bond distance (Å)		Atom name	Bond distance (Å)	
	Calculated	Experimental		Calculated	Experimental
C1-C2	1.391	1.393	C7-C8	1.479	1.476
C1-C6	1.392	1.369	C8-C9	1.349	1.349
C1-H1	1.082	0.930	C8-H5	1.082	0.930
C2-C3	1.394	1.389	C9-C10	1.442	1.444
C2-Cl1	1.755	1.737	C9-H6	1.087	0.930
C3-C4	1.388	1.394	C10-C11	1.382	1.649
C3-H2	1.083	0.930	C10-S1	1.753	1.438
C4-C5	1.402	1.400	C11-C12	1.415	1.687
C4-H3	1.083	0.930	C11-H7	1.082	0.931
C5-C6	1.401	1.402	C12-C13	1.372	1.371
C5-C7	1.503	1.495	C12-H8	1.082	0.930
C6-H4	1.082	0.930	C13-S1	1.723	1.636
C7-O1	1.225	1.231	C13-H9	1.079	0.931

Atom name	Bond angle (°)		Atom name	Bond angle (°)	
	Calculated	Experimental		Calculated	Experimental
C2-C1-C6	119.1	118.67	C11-C10-S1	109.9	114.01
C1-C2-C3	121.2	121.82	C10-C11-C12	113.6	94.45
C1-C2-Cl1	119.4	119.15	C3-C4-C5	121.2	119.10
C1-C6-C5	121.0	120.66	C4-C5-C6	118.5	119.66
C3-C2-Cl1	119.4	119.04	C4-C5-C7	117.7	122.26
C2-C3-C4	119.0	119.10	C6-C5-C7	123.8	118.07
O1-C7-C8	121.5	122.03	C5-C7-O1	119.6	119.68

[1] The experimental data presented here is taken from ref. [8].

C7-C8-C9	120.2	120	C5-C7-C8	118.9	118.29
C8-C9-C10	126.6	125.46	C10-S1-C13	92.0	96.92
C9-C10-C11	130.7	121.83	C11- C12-C13	112.8	111.34
C9-C10-S1	119.4	124.08	C12-C13-S1	111.7	123.1

Atom name	**Dihedral angle (°)**		**Atom name**	**Dihedral angle (°)**	
	Calculated	Experimental		Calculated	Experimental
C6-C5-C7-C8	-13.45	-27.58	C8-C9-C10-C11	-1.05	-12.01
C4-C5-C7-C8	167.8	155.39	C8-C9-C10-S1	178.97	171.40
C6-C5-C7-O1	167.2	152.83	H6-C9-C10-C11	178.87	171.41

Table 2: Calculated vibrational wavenumbers (in cm^{-1}), scaled values by the dual scale factor 0.98 (below 1800 cm^{-1}) and 0.987 (above 1800 cm^{-1}), experimental Raman for the wavenumber of bands in units of cm^{-1}, and mode description.

Mode	Y_{calc}	ω_{scal}	ω_{Raman}	ω_{IR}	Mode description
1	16	16			τ(structural)
2	23	23	21		τ(structural)
3	49	48	34/43/51		τ(structural)
4	79	77	60/79		τ(structural)
5	96	94	93/105		τ(structural)
6	124	122	124/139		τ(structural)
7	160	157	147/155		τ(structural)
8	195	191	196		τ(structural)
9	257	252			τ(structural)
10	275	270			τ(structural)
11	297	291	287		τ(structural)
12	326	319	323		τ(R1) + δ(C8C7O1)
13	367	360	361/376		τ(R1) + δ(S1C10C9)
14	417	409	396/417		γ(C1H1) + γ(C3H2) + γ(C4H3) + γ(C6H4)
15	477	467	464		τ(R1) + τ(R2) + γ(C8C7C5)
16	487	477	480		τ(R1) + τ(R2) + δ(C9C8H5)
17	497	487	485/500		τ(R1) + τ(R2) + δ(C9C8H5)
18	534	523	542		τ(R1-Cl) + τ(H5C8C7O1)
19	572	561	570		γ(C12H8) + γ(C11H7) + γ(C8H5)
20	588	576	579/592		Ring breath (R2)
21	643	630	622/628		Ring breath (R1)
22	690	676	679	673	γ(C1H1) + γ(C3H2) + γ(C8H5) + γ(C13H9) + γ(C8C7C5)
23	702	688	697	706	δ(S1C10C11) + δ(C8C7O1) + δ(R1)
24	712	698	716		γ(C11H7) + γ(C12H8) + γ(C13H9)
25	745	730	724		τ(R2)
26	753	738	741/748	737	τ(C8-C7-C5) + γ(C8H5) + γ(C6H4) + γ(C4H3)
27	768	753	756	754	Ring breath (R1 + R2)
28	831	814		818	γ(C6H4) + γ(C4H3) + γ(C11H7) + γ(C8H5)
29	835	818		836	γ(C13H9) + γ(C12H8) + γ(C11H7) + γ(C4H3) + γ(C3H2) + γ(C6H4) + γ(C1H1)
30	850	833		857	γ(C4H3) + γ(C3H2) + γ(C8H5)
31	864	847			δ(R2)
32	885	867	874	873	γ(C3H2) + γ(C8H5)
33	901	883			δ(C9C8C7) + δ(C11H7) + δ(C5C4C3)
34	920	902	892	889/912	γ(C13H9) + γ(C12H8) + γ(C11H7)
35	966	947		955	γ(C6H4) + γ(C1H1) + γ(C4H3)
36	999	979	979	970	γ(C4H3) + γ(C3H2)
37	1009	989	1013	1006	γ(C9H6) + γ(C8H5)
38	1023	1003	1029	1031	δ(C6C5C4) + δ(C1C2C3) + δ(H5C8C7) + δ(C12H8)
39	1035	1014	1036		δ(C6C5C4) + ν(C8C7) + δ(C12H8) + δ(C11H7)
40	1067	1046	1045	1049	δ(C12H8) + δ(C11H7)
41	1100	1078	1078	1076	δ(C4H3) + δ(C3H2) + δ(C1H1) + δ(C6H4) + ν(C2Cl1)
42	1102	1080			δ(C13H9) + δ(C12H8)
43	1131	1108	1092	1109	δ(C4H3) + δ(C3H2) + δ(C1H1) + δ(C6H4)
44	1151	1128	1135	1130	δ(C10C11H7) + δ(C12H8) + δ(C9H6) + δ(C8H5) + δ(C13H9) + δ(C4H3)
45	1201	1177	1179	1179	δ(C4H3) + δ(C3H2) + δ(C1H1) + δ(C6H4)
46	1227	1202	1194	1194	δ(C9H6) + δ(C8H5) + δ(C6H4) + δ(C3H2) + ν(C7C5)
47	1272	1247	1216	1210	δ(C13H9) + δ(C12H8) + δ(C11H7)
48	1317	1291	1222	1236	δ(C9H6) + δ(C8H5) + δ(C6H4) + δ(C3H2)

Mode	Y_{calc}	ω_{scal}	ω_{Raman}	ω_{IR}	Mode description
49	1324	1298	1283	1278	δ(C8H5) + ν_{R1}(C-C) + δ(C3H2) + δ(C4H3) + δ(C6H4)
50	1339	1312	1297	1306	δ(C9H6)
51	1357	1330	1310	1323	δ(C8H5) + δ(C3H2) + δ(C4H3) + δ(C6H4)
52	1390	1362	1361	1358/1366	ν_{R1}(C=C) + δ(C11H7) + δ(C12H8) + δ(C13H9) + δ(C9H6) + δ(C13-S1-C10)
53	1426	1397	1417	1421	ν_{R2}(C=C) + δ(C3H2) + δ(C4H3) + δ(C6H4) + δ(C1H1)
54	1453	1424	1425		ν_{R2}(C=C) + δ(C11H7) + δ(C12H8)
55	1516	1486	1489	1484	ν_{R1}(C=C) + δ(C3H2) + δ(C4H3) + δ(C6H4) + δ(C1H1)
56	1557	1526	1518		ν_{R2}(C=C) + δ(C11H7) + δ(C12H8) + δ(C13H9) + δ(C9H6)
57	1600	1568	1518	1510	ν_{R1}(C=C) + δ(C3H2) + δ(C4H3) + δ(C6H4) + δ(C1H1) + ν(C7=O1)
58	1620	1588	1569	1565	ν(C9-C8) + δ(C8H5) + δ(C9H6) + ν(C7=O1) + ν_{R1}(C=C) + δ(C3H2) + δ(C4H3) + δ(C6H4) + δ(C1H1)
59	1629	1596	1591/1584	1582	ν(C9-C8) + δ(C8H5) + δ(C9H6) + ν(C7=O1) + ν_{R1}(C=C) + δ(C3H2) + δ(C4H3) + δ(C6H4) + δ(C1H1)
60	1709	1675	1653	1652	ν(C9-C8) + δ(C8H5) + δ(C9H6) + ν(C7=O1)
61	3150	3024			ν(C9H6)
62	3185	3058	3059		ν(C8H5) + ν(C6H4) + ν(C1H1)
63	3194	3066			ν(C4H3) + ν(C3H2)
64	3197	3069			ν(C12H8) + ν(C11H7) + ν(C8H5) + ν(C6H4) + ν(C1H1)
65	3201	3073	3074	3075	ν(C12H8) + ν(C11H7) + ν(C8H5) + ν(C6H4) + ν(C1H1)
66	3206	3078		3080	ν(C4H3) + ν(C3H2)
67	3208	3080	3086	3083	ν(C12H8) + ν(C11H7) + ν(C8H5) + ν(C6H4) + ν(C1H1)
68	3214	3085	3109	3100	ν(C13H9) + ν(C12H8) + ν(C11H7)
69	3245	3115	3111	3200	ν(C13H9)

Nomenclature: τ = torsion; δ = bending; γ = out of plane bending; ν = stretching; R1 = benzene ring; R2 = thiophen ring.

Graphical Abstract

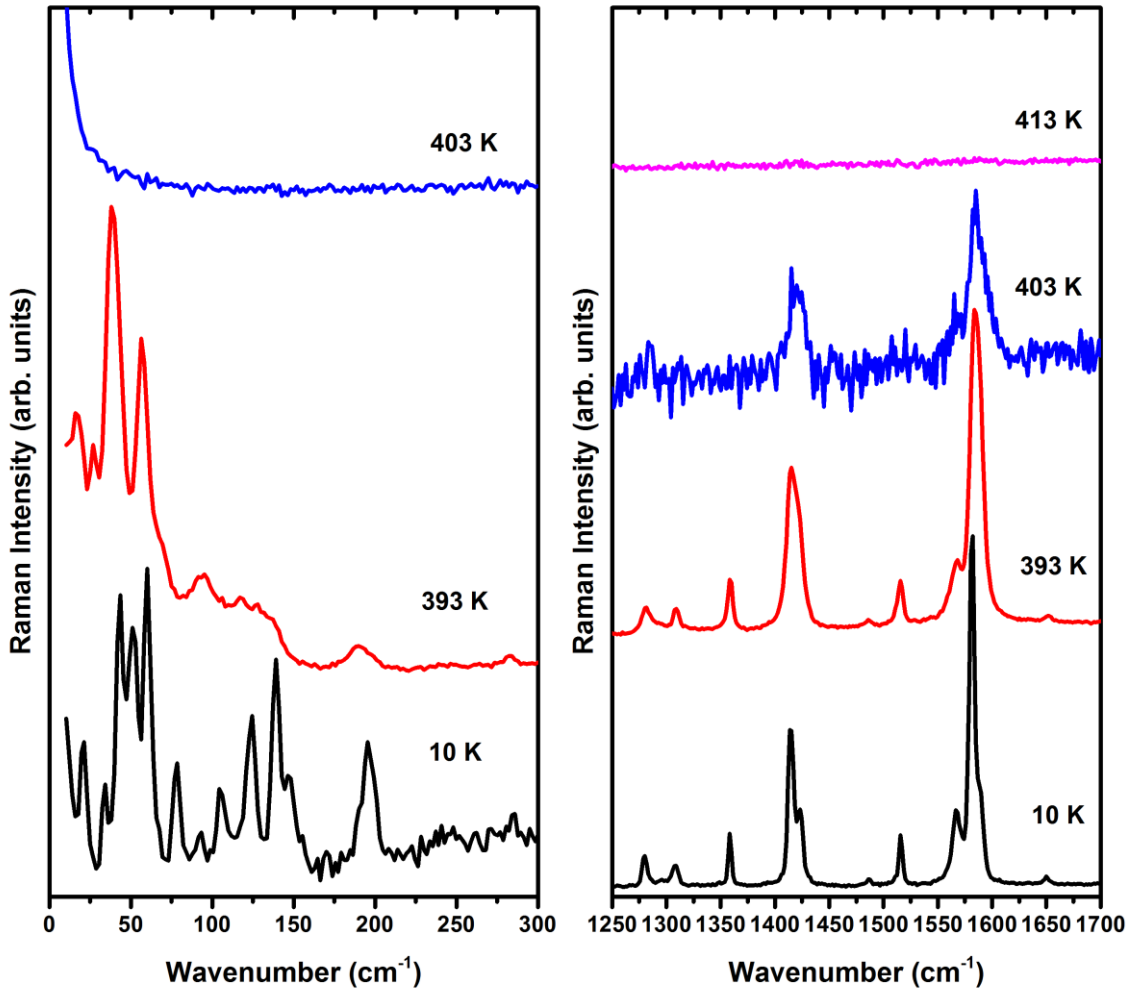

Highlights

- Physical characterization of heterocyclic chalcone containing thiophene ring.
- It is presented temperature dependence on Raman spectra of 1-(4-chlorophenyl)-3-(thiophen-2-yl)prop-2-en-1-one.
- DFT calculations were performed to supported experimental results.